

The density profile of Milky Way dark matter halo constrained from the OGLE microlensing sky map

S. Lin¹, W. Luo^{2,1}, Y.F. Cai^{1,2}, Q. Guo¹, L. Wei³, B. Wang¹, Q. Li⁴, C. Su¹ and A. Rodriguez⁵

¹ Department of Astronomy, School of Physical Science, University of Science and Technology of China, Hefei, Anhui 230026, China

² Institute of Deep Space Sciences, Deep Space Exploration Laboratory, Hefei, 230026, China

³ School of Physics and Astronomy, Sun Yat-sen University, 2 Daxue Road, Zhuhai 519082, China

⁴ Department of Physics and Astronomy, University of Utah, Salt Lake City, UT 84102, USA

⁵ Department of Astronomy, University of Michigan, 1085 S. University, Ann Arbor, MI 48109 e-mail: all2b9s@mail.ustc.edu.cn
e-mail: wtluo@ustc.edu.cn

Received September 29, 2024; accepted November 21, 2024

ABSTRACT

We report the detection of a 282^{+34}_{-31} pc-sized core in the center of Milky Way dark matter halo at 68% confidence level by using the micro-lensing event rate sky map data from the Optical Gravitational Lensing Experiment (OGLE) survey. We apply the spacial information of the microlensing sky map and model it with the detailed Milky Way dark matter halo Core/Cusp profile, and the fraction of dark matter in the form of Mini Dark Matter Structure (MDMS, $f_{\text{MDMS}} = \Omega_{\text{MDMS}}/\Omega_{\text{DM}}$), e.g. primordial black hole, earth-mass subhalos, floating planets and so on. We find that this sky map can constrain both f_{MDMS} and the core size simultaneously without strong degeneracy while fully considering mass function of Milky Way stellar components from both the bulge and disk.

Key words. dark matter – Galaxy: halo – Gravitational lensing: micro

1. Introduction

The concordance cosmology is such a successful model that it fits most of the observations with only half a dozen parameters, e.g. Cosmic Microwave Background (CMB) Planck Collaboration et al. (2020), Supernova Ia (SNIa) Riess et al. (1998), time delay projects based on strongly lensed Active Galactic Nuclei (AGNs) Birrer et al. (2020), and weak lensing statistics Hikage et al. (2019). However, despite all these successes, tensions emerge among different cosmological probes, e.g. the recent Hubble tension between the Planck observation and SNIa Verde et al. (2019), the “lensing is low” issue on cosmological parameters between weak-lensing measurements and CMB Leauthaud et al. (2017).

At small scales, there exist a series of “crises” as well, including the missing satellite problem (MSP), too big to fail (TBTf), as well as the core-cusp problem (CCP) de Blok (2010). Especially, the core-cusp issue, where the inferred dark matter core structure from nearby dwarf galaxies contradicts the Navarro-Frenk-White (NFW) profile, a cuspy profile from pure cold dark matter simulations Navarro et al. (1997), leads to the extensive study on the formation mechanism of the core structure either from an exotic self interacting dark matter (SIDM) model Spergel & Steinhardt (2000); Jiang et al. (2023), or an astrophysical model from baryonic feedback and merging, dynamical friction, e.t.c. [see review papers of Salucci (2019); Del Popolo & Le Delliou (2022)]. Moreover, the enigmatic Gould Belt can be created by a “dark matter core” colliding with the gas disk of Milky Way Diemand et al. (2008); Bekki (2009). However, so far there is no conclusive observational evidence to either confirm or reject the aforementioned core structure of Milky Way.

This is largely due to the fact that dark matter itself can not be directly observed and the rotation curve of Milky Way is not as informative as nearby dwarf galaxies Gentile et al. (2004); Bekki (2009); Karukes & Salucci (2017). New probes are then necessary for mapping the dark side of the Milky Way and comparing them to simulations, which will boost our understanding of the core formation of Milky Way halo and the like.

The method we develop here is based on the assumption that a fraction of dark matter are in the form of primordial black holes Novikov et al. (1979); Carr & Kühnel (2020); Sasaki et al. (2018), dark matter halos with hundreds of earth masses Wang et al. (2020), or to a very recent work Delos & Silk (2023): the so-called dark matter minihalos with extremely high internal density of $10^{12} M_{\odot}/\text{pc}^3$. We generalize it as mini dark matter structures (MDMS) which follow the density profile of Milky Way dark matter halo and can induce the micro-lensing event when intervening the line between the background star and the observer.

Fig.1 presents the patterns of micro-lensing event rate map between the cuspy NFW profile (left panel) and the cored density profile (middle panel). The right panel is the event rate sky map of OGLE newest data release Mróz et al. (2019). By fitting the OGLE sky map, we can constrain the dark matter density profile.

Here, we serendipitously found that the spatial distribution of micro-lensing event rate sky map targeting the Galactic center from Optical Gravitational Lensing Experiment (OGLE) Mróz et al. (2020) can put strong constraints simultaneously on both Mini Dark Matter Structures (MDMS) fraction, and the core size of the central part of Milky Way dark matter halo. The inferred size of the dark core is 282^{+34}_{-31} pc at 68% confidence level. Further, this result can put constraints on both dark matter models

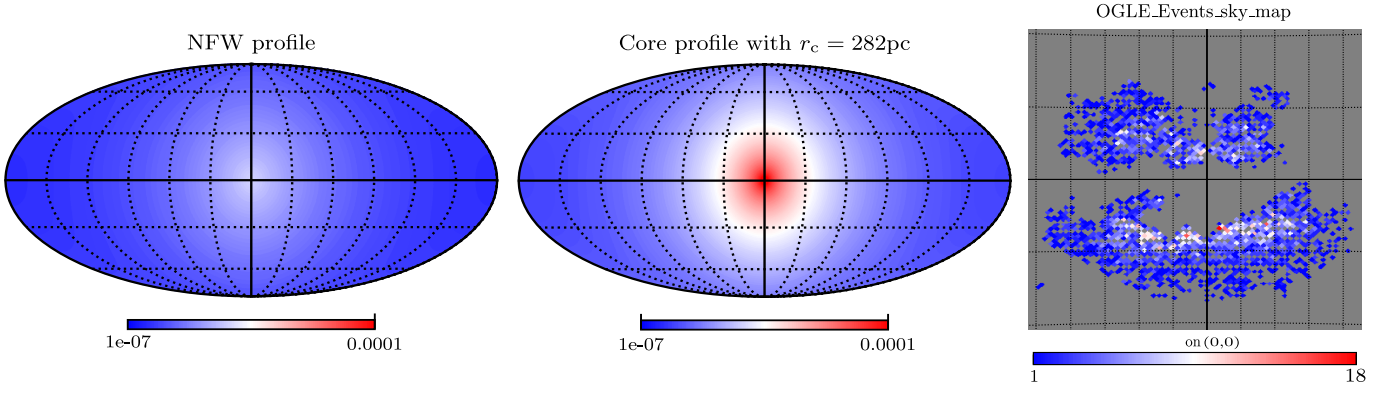


Fig. 1. The sky-maps are plotted in Mollweide projection. Left panel: Micro-lensing event rate given an NFW density profile; Middle panel: 282pc core size event rate; Right panel: The sky map of 5790 OGLE micro-lensing events. The difference between graticules are 2 degrees in longitude and 4.5 degrees in latitude. As we are unable to reach all the detailed data of micro-lensing events used to build the catalog, we can not plot an event-rate sky map [Readers can find it in Fig.24 of Mróz et al. (2020)].

beyond cold dark matter (CDM) or the baryonic physics of the Milky Way Wetzel et al. (2023). Either way, this discovery opens another window to peek at the mystery of the core-cusp problem.

2. Microlensing model

Our model extends the micro-lensing geometry and notations in Niikura et al. 2019 Niikura et al. (2019) by fully employing the spacial information. We take the x -direction to be along the line connecting the Galactic center and the Earth (the observer's position), with the assumption that the Earth is located at $(x, y, z) = (8\text{kpc}, 0, 0)$. And the y -direction is the rotating direction of the Earth in the Galactic disk plane together with the z -direction being perpendicular to the plane.

In this paper, we denote the mass of the lens as M , while the source-observer, lens-observer, and source-lens distance as d_s , d_l and $d_{ls} = d_s - d_l$. In our coordinate system, a lens at d_l will be located at: $x = 8\text{kpc} - d_l \cos l \cos b$, $y = d_l \cos b \sin l$, $z = d_l \sin b$. As the OGLE survey mainly focuses on the source near the Galactic center, we assume $d_s = 8\text{kpc}$ for all the sources as have been done in Niikura et al. 2019 Niikura et al. (2019). With the above notation, the Einstein radius R_E for a given mass M can be expressed as:

$$R_E = \sqrt{\frac{4GM d_l d_{ls}}{c^2 d_s}} \quad (1)$$

For simplicity, we consider that all the lenses have an identical mass of M for MDMS, but stellar mass function (see the following section) for bulge and disk contribution. Both of them follow the Maxwell-Boltzmann velocity distribution (we also test a different velocity distribution to examine if the core size varies accordingly in the supplemental appendix). To be specific, as we are only interested in the relative velocity between lenses and source that is perpendicular to the x direction, the velocity distribution has the following form:

$$f(\mathbf{v}_\perp) = \frac{1}{2\pi\sigma_y\sigma_z} \exp\left[-\frac{(v_\perp \cos\theta - \bar{v}_y)^2}{\sigma_y^2} + \frac{(v_\perp \sin\theta - \bar{v}_z)^2}{\sigma_z^2}\right] \quad (2)$$

where θ represents the direction of \mathbf{v}_\perp , σ_y , σ_z are the velocity dispersion of lens in the y and z directions and \bar{v}_y , \bar{v}_z are the mean velocity along y and z directions.

With the above assumptions, the micro-lensing event rate for timescale t_E along a certain direction is then:

$$\frac{d\Gamma_d}{dt_E} = \pi \int d(\ln M) \frac{dn_{\text{lens}}(M)}{d \ln M} \int_0^{d_s} dd_l \frac{\rho_{\text{lens}}(d_l)}{M} \int_{-\pi/2}^{\pi/2} d\theta v_\perp^4 f_{\text{lens}}(v_\perp, \theta) \quad (3)$$

where t_E is the microlensing event time scale given by $t_E = (2R_E \cos\theta)/(v_\perp)$. And $\rho_{\text{lens}}(d_l)$ is the density profile for lenses' distribution along the line of sight at the distance of d_l , whose specific expression depends on its kind, i.e. dark matter, bulge stellar and disk stellar. The ρ_{lens} of MDMS can be simply expressed as $f_{\text{MDMS}}\rho_{\text{halo}}$, and $f_{\text{MDMS}} = \frac{\Omega_{\text{MDMS}}}{\Omega_{\text{DM}}}$ denoting the fraction of MDMS as dark matter. The term in the right side of Eq.3 $\frac{dn_{\text{lens}}(M)}{d \ln M}$ is the mass function of lens. We assume a delta mass function for MDMS and will discuss the detailed mass function of stellar components in the following sections.

As the density profile is only considered in the integration along the line of sight, the angular distribution of the density profile is encoded inside the event rate distribution.

2.1. Dark matter profile

For cusp-like dark matter halo, we adopt the NFW density profile:

$$\rho_{\text{NFW}}(r) = \frac{\rho_c}{(r/r_s)(1+r/r_s)^2} \quad (4)$$

where r is the distance to the Galactic center, $\rho_c = 4.88 \times 10^6 M_\odot/\text{kpc}^3$ and $r_s = 21.5\text{kpc}$. For a core-liked halo, we choose the Burkert density profile Burkert (1995); Salucci & Burkert (2000):

$$\rho_{\text{BK}}(r) = \frac{\rho_b}{(1+r/r_b)(1+(r/r_b)^2)} \quad (5)$$

where r_b stands for the core size and ρ_b is determined by the halo mass. Here we assume the Milky Way halo mass to be of $10^{12} M_\odot$ Klypin et al. (2002). The density profile and velocity profile we use for each component of lens are shown in Table.1 Niikura et al. (2019).

Lens' kind	Density profile $\rho[M_\odot/\text{pc}^3]$	Velocity profile(μ, σ) [km/s]
Bulge	$1.04 \times 10^6 (\frac{s}{0.482\text{pc}})^{-1.85}, (s < 938\text{pc})$	$f_y : \{-220(1 - \alpha), 100 \sqrt{1 + \alpha^2}\}$
	$3.53 K_0(\frac{s}{667\text{pc}}), (s \geq 938\text{pc})$	$f_z : \{0, 100 \sqrt{1 + \alpha^2}\}$
Disk	$0.06 \times \exp[-\{\frac{R-8000}{3500} + \frac{z}{325}\}]$	$f_y : \{220\alpha, \sqrt{(\kappa\delta + 30)^2 + (100\alpha)^2}\}$
		$f_z : \{0, \sqrt{(\lambda\delta + 30)^2 + (100\alpha)^2}\}$
MDMS	Cusp: $4.88 \times 10^{-3} \frac{1}{(r/r_s)(1+r/r_s)^2}$	$f_y : \{-220(1 - \alpha), \sqrt{220^2 + (100\alpha)^2}\}$
	Core: $\frac{\rho_b}{(1+r/r_b)(1+(r/r_b)^2)}$	$f_z : \{0, \sqrt{220^2 + (100\alpha)^2}\}$

Table 1. Density profile and velocity profile for each kind of lens, where $\alpha = d_1/d_s$, $\kappa = 5.625 \times 10^{-3} \text{km/s/pc}$, $\lambda = 3.75 \times 10^{-3} \text{km/s/pc}$, $\delta = (8000 - x)\text{pc}$, $K_0(x)$ is modified Bessel function and $R = (x^2 + y^2)^{1/2}$, $s^4 = R^4 + (z/0.61)^4$, $r^2 = x^2 + y^2 + z^2$

2.2. Mass function of stellar components

In order to estimate the event rate of stellar components in bulge and disk, we need to get the mass function of each kind. For this purpose, we assume the Kroupa broken power-law initial mass function (IMF) Kroupa (2001).

$$\frac{dn_s(M)}{d \ln M} = \begin{cases} A_{\text{MS}} \left(\frac{M}{M_{\text{break}}}\right)^{-\alpha_{\text{MS1}}} & (M \leq M_{\text{break}}) \\ A_{\text{MS}} \left(\frac{M}{M_{\text{break}}}\right)^{-\alpha_{\text{MS2}}} & (M \geq M_{\text{break}}) \end{cases} \quad (6)$$

Following previous work Niikura et al. (2019), we assume all stars within the initial mass range [$1 \leq M_{\text{break}}/M_\odot \leq 8$] evolves into White Dwarfs following initial-final mass relation of $M_{\text{WD}} = 0.339 + 0.129M_{\text{init}}$ and stars with [$8 \leq M_{\text{break}}/M_\odot \leq 20$] into neutron stars following a Gaussian distribution with mean value $M_{\text{final}} = 1.39M_\odot$ and width $\sigma = 0.12M_\odot$.

We choose the newer data from Mróz et al. 2020 Mróz et al. (2020) instead of the previous version based on Mróz et al. 2017 Mróz et al. (2017) which only contains 9 fields. Here, we set $\alpha_{\text{MS2}} = 2$, $M_{\text{break}} = 0.5M_\odot$, and leave α_{MS1} as free parameter to be sampled by MCMC. We choose $\alpha_{\text{MS1}} = 1.1$ as fiducial value, which is consistent with result from Sagittarius Window Eclipsing Extrasolar Planet Search (SWEEPS) Calamida et al. (2015).

2.3. Fitting to data

Before proceeding with MCMC, we need to subtract the contribution of bulge and disk components in event rates sky map. That is:

$$\Gamma_{\text{fixed},k} = \Gamma_{\text{OGLE},k} - \Gamma_{\text{bulge},k} - \Gamma_{\text{disk},k} \quad (7)$$

where k is the index of fields in OGLE survey Mróz et al. (2020). Afterwards, we neglect all the fields with negative values and use the remaining 55 fields, where we choose to fit two variables: the fraction of MDMS (f_{MDMS}) and the size of the core ($\log_{10} r_b$) by fitting the theoretical event rate Γ_{Core} to the event rate at the directions of 55 fields. For simplicity, we assume a log-normal likelihood function:

$$\ln(p) = \sum_{k=1}^{55} -\frac{(\ln(\Gamma_{\text{Core},k}) - \ln(\Gamma_{\text{fixed},k}))^2}{2\sigma_k^2} + \ln(\sigma_k) \quad (8)$$

σ_k in the above formula is given by $\sigma_k^2 = \ln(1 + \sigma_{\text{OGLE},k}^2/\Gamma_{\text{fixed},k}^2)$ in which $\sigma_{\text{OGLE},k}$ is the error of event rate from the OGLE data.

Based on the likelihood function, we use the python package EMCEE Foreman-Mackey et al. (2013) to run MCMC with 20 walkers and 3500 steps each after burn-in processes of 500 steps. The posteriors of the two parameters are therefore sampled from the chains.

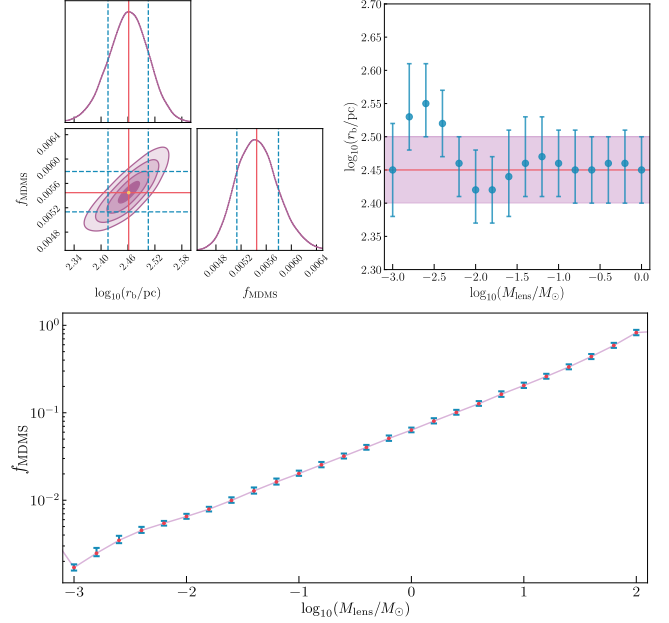


Fig. 2. Top left: The corner plot of the two parameters f_{MDMS} and core size r_b with lens mass of $10^{-2.2}M_\odot$. The red solid lines are the median value of the posterior distribution and the blue dashed lines denote the 68% confidence interval. The yellow point is the median value of MCMC sampled posterior and different contours in the corner plot denote the different σ levels.

Top right: The core size as a function of lenses' mass. The red solid line is the median value from the left panel for r_b with one sigma range as the purple belt. The different core sizes sampled from different lens mass is shown as the data points with error bars. The value remains almost unchanged within one sigma level.

Bottom: Fraction of MDMS f_{MDMS} from MCMC as function of lenses' mass. The red points are the median with blue errorbars showing the one sigma range for each mass value. The purple solid line connects the median values.

3. Results

We perform a test by calculating the Bayesian factor for both the cuspy profile (NFW formula) and the core profile (Burkert formula) with the nested sampling Monte Carlo algorithm MLFriends Buchner (2016, 2019) using the UltraNest package Buchner (2021). For all the lens mass we tested, the ratios between Bayesian factors of the Burkert profile and NFW profile are larger than 10^3 . This illustrates that the Burkert density profile is much more probable than the NFW profile.

The major results are shown in Fig.2, the top left panel presents the posterior distribution of core size ($\log_{10}(r_b/\text{pc})$) and the fraction of MDMS (f_{MDMS}) assuming the lens mass of

$\sim 10^{-2}M_{\odot}$. The latter varies significantly as a function of lens mass due to the OGLE survey cadence (the bottom panel of Fig.2). Nonetheless, the core size remains consistent with the fiducial value that the lens is set to be one solar mass (red solid line with one sigma pink shaded region in the top right panel of Fig.2). The effective range is between $10^{-3}M_{\odot}$ and 10^0M_{\odot} , where the constraint is the most effective based on OGLE survey data.

Astonishingly, for lens' mass around $10^{-3}M_{\odot}$, f_{MDMS} is about 10^{-3} . That means, to the maximum, 10^9M_{\odot} dark matter is in the form of MDMS, which is a much stronger constraint than previous result (Niikura et al. 2019). The dependence of f_{MDMS} on lens mass is due to the cadence of OGLE survey which is in [0.1days, 300days]. As a result, when lens' mass is too large ($> 1M_{\odot}$) or too small ($< 10^{-3}M_{\odot}$), the constraint on f_{MDMS} is approaching to 1. The bottom panel of Fig.2 clearly shows the dependence of f_{MDMS} on lens stellar mass, which is purely introduced by the OGLE survey cadence.

4. Discussion and summary

In a review on the density profile of dark matter halos by Paulo Salucci et al 2019 (Salucci 2019) concludes that the Milky Way dark matter halo has a core structure with the size between 1-100kpc. Nesti & Salucci (2013) estimated the core size of Milky Way dark matter halo to be about 10kpc using multiple dynamical data, such as MW terminal velocities in the region inside the solar circle, circular velocity as recently estimated from maser star forming regions at intermediate radii, and velocity dispersions of stellar halo tracers for the outermost Galactic region. The relation between our result and theirs is worth being probed if the smaller structure is an additional one besides the larger core.

In Chan et al. (2015), they generate a suite of simulations based on the same code of FIRE, focusing on the core size of galaxies with a wide range of stellar mass and feedback. Their results present much larger core sizes than ours ranging from 1.2kpc to 2.0kpc for Milky Way dark matter halo. Our results shows a much smaller core size that caused by the baryonic feedback in those simulations.

As the first try to constrain the core of Milky Way dark matter halo using the OGLE micro-lensing sky map, we do realize the limitation of the OGLE data for our constraints, which is targeting the Milky Way bulge. Before we draw any solid conclusion of the implications for hydro simulations and dark matter particle properties (as described in the next paragraph) with the core size, we will further explore other means to test our results. In an another upcoming work, we select micro-lensing event candidates in Milky Way halo using a technique called "static micro-lensing" (Guo et al. (2024), He et al in prep.). We will further explore the core size based on those new data. In future, powerful time domain surveys such as LSST Ivezić et al. (2019), WFST (Wang et al. 2023) will also provide valuable microlensing events in Milky Way halo.

On the other hand, phenomenological models beyond CDM provide another means to interpret the core structure formation, ranging from a solitonic core of ultra-light dark matter (ULDM) Kendall & Easther (2020), or fuzzy dark matter (FDM) Burkert (2020), to self-interacting dark matter (SIDM) Rocha et al. (2013a) as well as weakly interacting massive particles (WIMP) de Swart et al. (2017). However, the core size of the dark matter halo behaves differently in the stellar feedback scenario from one those models, specifically SIDM model Rocha et al. (2013b). The former shows the core size peaks around $\log_{10}(M_*/M_{\odot}) \sim 10.0$

while the latter illustrates a monotonic increase as a function of halo mass. In general, different dark matter particle models can potentially be tested by astrophysical observations, such as modulated Einstein rings from multiple image systems of strong-lensing events Amruth et al. (2023). We present a novel method to probe the dark matter density profile by using the microlensing sky map, which can be used to further constrain various mechanisms of core formation.

To summarize, we apply the OGLE micro-lensing sky map to obtain by far the tightest constraint on the core size of Milky Way dark matter halo. The core size value is 282^{+34}_{-31} pc and is independent of M_{lens} within a wide mass range. This result can potentially put stronger constraints on the cross section of SIDM particles, the mass of ULDM/FDM. The core size can constrain the strength of star formation process of Milky Way. We acknowledge that we do not consider an off-center between the dark matter halo potential center and the Galactic center in our modeling which can be another interesting issue to probe. We also notice that the OGLE event rate sky map we use only locates at the Galactic center, and more data beyond the Galactic center region will greatly improve the constraint based on our model.

In the future, providing a wider range survey of microlensing event rate map (potentially Gaia archive data Gaia Collaboration et al. (2021)), or novel statistical measures of microlensing event rate sky map, our method can be extended to a series of studies on the detailed structures of Milky Way dark matter halo.

We are grateful to Shude Mao, Ruizhi Yang, Weicheng Zang, Elisa Ferreira, and Christopher J. Miller for valuable discussions. This work is supported in part by NSFC (12192224, 12003029, 11833005), National Key R&D Program of China (2021YFC2203100), the Frontier Scientific Research Program of Deep Space Exploration Laboratory (No. 2022-QYKYJH-HXYF-012), by CAS young interdisciplinary innovation team (JCTD-2022-20), by 111 Project for "Observational and Theoretical Research on Dark Matter and Dark Energy" (B23042), by Fundamental Research Funds for Central Universities, by CSC Innovation Talent Funds, by USTC Fellowship for International Cooperation, by USTC Research Funds of the Double First-Class Initiative, by CAS project for young scientists in basic research (YSBR-006).

Data availability. The code supporting this work is available from the corresponding authors upon reasonable request.

The EMCEE package is available under MIT License in: <https://emcee.readthedocs.io/en/stable/>.

The Ultranest package is available in <https://johannesbuchner.github.io/UltraNest/>.

The microlensing modeling code is available in <https://github.com/all2b9s/Static-microlensing>.

The OGLE catalogue is publicly available in: <https://ogle.astrouw.edu.pl/>.

References

- Amruth, A., Broadhurst, T., Lim, J., et al. 2023, *Nature Astronomy*, 7, 736
- Bekki, K. 2009, *Monthly Notices of the Royal Astronomical Society: Letters*, 398, L36
- Birrer, S., Shajib, A. J., Galan, A., et al. 2020, *Astronomy & Astrophysics*, 643, A165
- Bozorgnia, N. & Bertone, G. 2017, *International Journal of Modern Physics A*, 32, 1730016
- Buchner, J. 2016, *Statistics and Computing*, 26, 383

- Buchner, J. 2019, *Publications of the Astronomical Society of the Pacific*, 131, 108005
- Buchner, J. 2021, *The Journal of Open Source Software*, 6, 3001
- Burkert, A. 1995, *The Astrophysical Journal*, 447
- Burkert, A. 2020, *The Astrophysical Journal*, 904, 161
- Calamida, A., Sahu, K. C., Casertano, S., et al. 2015, *The Astrophysical Journal*, 810, 8
- Carr, B. & Kühnel, F. 2020, *Annual Review of Nuclear and Particle Science*, 70, 355
- Chan, T. K., Kereš, D., Oñorbe, J., et al. 2015, *Monthly Notices of the Royal Astronomical Society*, 454, 2981
- Croon, D., McKeen, D., & Raj, N. 2020, *Physical Review D*, 101
- de Blok, W. J. G. 2010, *Advances in Astronomy*, 2010, 789293
- de Swart, J. G., Bertone, G., & van Dongen, J. 2017, *Nature Astronomy*, 1, 0059
- Del Popolo, A. & Le Delliou, M. 2022, arXiv e-prints, arXiv:2209.14151
- Delos, M. S. & Silk, J. 2023, *Monthly Notices of the Royal Astronomical Society: Letters*, 520, 4370
- Diemand, J., Kuhlen, M., Madau, P., et al. 2008, *Nature*, 454, 735
- Foreman-Mackey, D., Hogg, D. W., Lang, D., & Goodman, J. 2013, *Publications of the Astronomical Society of the Pacific*, 125, 306
- Gaia Collaboration, Brown, A. G. A., Vallenari, A., et al. 2021, *Astronomy & Astrophysics*, 649, A1
- Gentile, G., Salucci, P., Klein, U., Vergani, D., & Kalberla, P. 2004, *MNRAS*, 351, 903
- Guo, Q., Wei, L., Luo, W., et al. 2024, arXiv e-prints, arXiv:2411.02161
- Hikage, C., Oguri, M., Hamana, T., et al. 2019, *Publications of the Astronomical Society of Japan*, 71, 43
- Ivezić, Ž., Kahn, S. M., Tyson, J. A., et al. 2019, *The Astrophysical Journal*, 873, 111
- Jiang, F., Benson, A., Hopkins, P. F., et al. 2023, *MNRAS*, 521, 4630
- Karukes, E. V. & Salucci, P. 2017, *PublicMonthly Notices of the Royal Astronomical Societyations of the*, 465, 4703
- Kendall, E. & Easther, R. 2020, *Publications of the Astronomical Society of Australia*, 37, e009
- Klypin, A., Zhao, H., & Somerville, R. S. 2002, *The Astrophysical Journal*, 573, 597
- Kroupa, P. 2001, *Monthly Notices of the Royal Astronomical Society*, 322, 231
- Leauthaud, A., Saito, S., Hilbert, S., et al. 2017, *Monthly Notices of the Royal Astronomical Society*, 467, 3024
- Mao, S. & Paczyński, B. 1996, *The Astrophysical Journal*, 473, 57
- Mao, Y.-Y., Strigari, L. E., Wechsler, R. H., Wu, H.-Y., & Hahn, O. 2013, *The Astrophysical Journal*, 764, 35
- Mróz, P., Udalski, A., Skowron, J., et al. 2017, *Nature*, 548, 183
- Mróz, P., Udalski, A., Szymański, M. K., et al. 2020, *The Astrophysical Journals*, 249, 16
- Mróz, P., Udalski, A., Skowron, J., et al. 2019, *The Astrophysical Journal Supplement Series*, 244, 29
- Navarro, J. F., Frenk, C. S., & White, S. D. M. 1997, *The Astrophysical Journal*, 490, 493
- Nesti, F. & Salucci, P. 2013, *J. Cosmology Astropart. Phys.*, 2013, 016
- Niikura, H., Takada, M., Yokoyama, S., Sumi, T., & Masaki, S. 2019, *Physical Review D*, 99
- Novikov, I. D., Polnarev, A. G., Starobinskii, A. A., & Zeldovich, I. B. 1979, *Astronomy & Astrophysics*, 80, 104
- Planck Collaboration, Aghanim, N., Akrami, Y., et al. 2020, *Astronomy & Astrophysics*, 641, A6
- Riess, A. G., Nugent, P., Filippenko, A. V., Kirshner, R. P., & Perlmutter, S. 1998, *The Astrophysical Journal*, 504, 935
- Rocha, M., Peter, A. H. G., Bullock, J. S., et al. 2013a, *Monthly Notices of the Royal Astronomical Society*, 430, 81
- Rocha, M., Peter, A. H. G., Bullock, J. S., et al. 2013b, *Monthly Notices of the Royal Astronomical Society*, 430, 81
- Salucci, P. 2019, *A&A Rev.*, 27, 2
- Salucci, P. & Burkert, A. 2000, *ApJ*, 537, L9
- Sasaki, M., Suyama, T., Tanaka, T., & Yokoyama, S. 2018, *Classical and Quantum Gravity*, 35, 063001
- Spergel, D. N. & Steinhardt, P. J. 2000, *Physical Review Letters*, 84, 3760
- Verde, L., Treu, T., & Riess, A. G. 2019, *Nature Astronomy*, 3, 891
- Wang, J., Bose, S., Frenk, C. S., et al. 2020, *Nature*, 585, 39
- Wang, T., Liu, G., Cai, Z., et al. 2023, *Science China Physics, Mechanics, and Astronomy*, 66, 109512
- Wetzel, A., Hayward, C. C., Sanderson, R. E., et al. 2023, *The Astrophysical Journals*, 265, 44

Appendix A: Model dependencies

In this supplementary material, we will discuss the model dependency of core size and f_{MDMS} to show the robustness of our result.

A.1 Velocity distribution – In the main body of this paper, a Maxwell-Boltzmann distribution for MDMS is assumed. Still, as shown in cosmological simulations, there are other velocity distribution candidates Bozorgnia & Bertone (2017). So here we will discuss how different velocity distributions affect our results.

As shown in Mao et al, 1996Mao & Paczyński (1996), for lens with a given velocity $|\mathbf{v}|$, the asymptotic behaviors of the event rate are given by:

$$\frac{d\Gamma_d}{dt_E} \propto \begin{cases} \left(\frac{t_E}{t_m}\right)^2 & (t_E \ll t_m) \\ \left(\frac{t_E}{t_m}\right)^{-4} & (t_E \gg t_m) \end{cases} \quad (\text{A.1})$$

where the characteristic timescale is $t_m = \frac{R_E |d_1|=0.5d_s}{|\mathbf{v}|}$. If we take the velocity distribution of the lens into account, we would need to integrate over $|\mathbf{v}|$:

$$\frac{d\Gamma_d}{dt_E} \propto \begin{cases} t_E^2 \int_0^\infty \frac{v^2 dv}{t_m^2} f(v) & (t_E \ll t_m) \\ t_E^{-4} \int_0^\infty \frac{v^2 dv}{t_m^4} f(v) & (t_E \gg t_m) \end{cases} \quad (\text{A.2})$$

As the velocity only takes value inside a limited interval due to $f(v)$, the integrals hold asymptotically.

As we can see from Eq. A.2, for any given velocity distribution, it only results in an overall factor to the event rate for short-timescale and large-timescale events, which is independent of the angular position of the source. As the constraint of core size comes from the angular distribution of event rate, the velocity distribution will have no impact on the prediction of core size when the time scale of events is very short or very large. That is to say, the impact of velocity distribution on the prediction only comes from those events with $t_E \sim t_m$.

To demonstrate the impact of the velocity distribution, here we use the model given in Mao et al. (2013) for the test:

$$f(|\mathbf{v}|) = \begin{cases} A \exp(-|\mathbf{v}|/v_0)(v_{\text{esc}} - |\mathbf{v}|)^p, & 0 \leq |\mathbf{v}| \leq v_{\text{esc}} \\ 0, & \text{otherwise} \end{cases} \quad (\text{A.3})$$

The result is shown in FIG. A.1. As we can see, even though the new model has a different mean velocity and velocity dispersion, the one-sigma range still overlaps with the previous one. This indicates the robustness of our result.

A.2 Extended lens – For a point lens, the criterion for a micro-lensing event is:

$$\Delta_{\text{sl}} < R_E \quad (\text{A.4})$$

Here, Δ_{sl} is the distance between the lens and the projection of the source in the lens plane. R_E is the Einstein radius.

When $\Delta_{\text{sl}} = R_E$, the total magnification $\mu_T = 1.34$. If we keep this criterion, as shown in Croon et al, 2020Croon et al. (2020), the effect of an extended lens will result in an impact parameter $u_{1.34}$ which serves as a modifying factor to R_E . So, the micro-lensing event rate for extended will be:

$$\frac{d\Gamma_d}{dt_E} = \pi \int d(\ln M) \frac{dn_{\text{lens}}(M)}{d \ln M} \int_0^{d_s} dd_1 \frac{\rho_{\text{lens}}(d_1)}{M} \int_{-\pi/2}^{\pi/2} d\theta (v'_\perp)^4 f_{\text{lens}}(v'_\perp, \theta) \quad (\text{A.5})$$

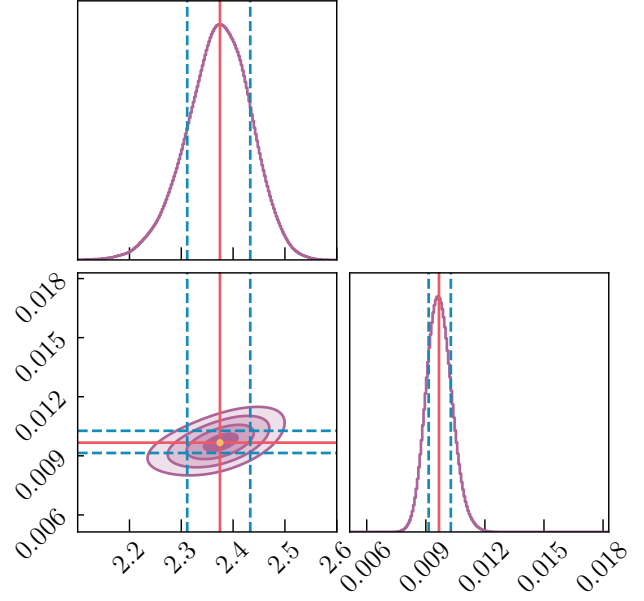


Fig. A.1. We use the velocity distribution given in Mao et al. (2013), with $(v_0/v_{\text{esc}}, p) = (0.13, 0.78)$ and $M_{\text{lens}} = 10^{-2.2} M_\odot$. Here the core size is 237^{+34}_{-32} ($2.37^{+0.06}_{-0.06}$ in magnitude) and the $f_{\text{MDMS}} = 0.0096^{+0.0006}_{-0.0005}$. The one-sigma range still overlaps with the Gaussian cases.

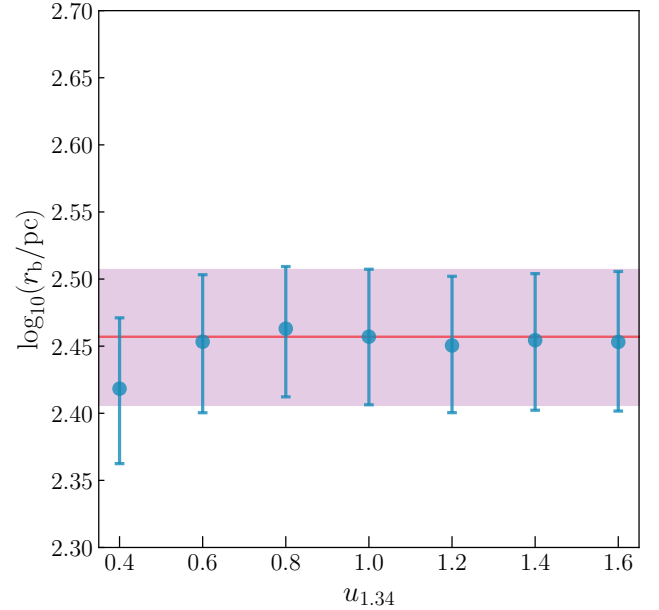


Fig. A.2. Here we have done tests with $u_{1.34} = 0.4, 0.6, 0.8, 1, 1.2, 1.4, 1.6$ and $M_{\text{lens}} = 10^{-1.0} M_\odot$. As we can see, for different impact parameters, the results are still within the one-sigma range of the fiducial value (i.e. $u_{1.34} = 1.0$.)

Here $v'_\perp = (2u_{1.34}R_E \cos \theta)/(t_E)$.

To test the impact of the possible extended structure of MDMS, we take $u_{1.34} = 0.4, 0.6, 0.8, 1, 1.2, 1.4, 1.6$ ($u_{1.34}$ is the case we showed in the main body of our paper) and rerun the whole analysis. The result is shown in FIG. A.2. For all the impact parameters we tested, the results are all within the one-sigma range of the point lens case (i.e. $u_{1.34} = 1.0$). This indicates that our result is still valid even when considering the extended structure of MDMS.

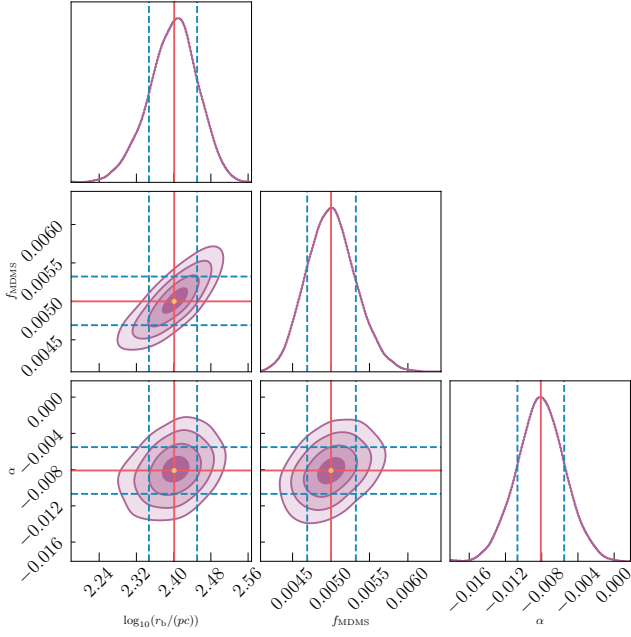


Fig. A.3. We use ρ_{aniso} defined in Eq. A.6 to rerun the MCMC with α as an additional parameter. Here, $M_{\text{lens}} = 10^{-2.2} M_{\odot}$. The core size is 252^{+30}_{-30} ($2.40^{+0.05}_{-0.05}$ in magnitude), $f_{\text{MDMS}} = 0.0050^{+0.0003}_{-0.0003}$, and $\alpha = -0.008^{+0.002}_{-0.002}$. This is still within the one-sigma range shown in the main body of our paper.

A.3 Anisotropy of density profile – As discussed in Mróz et al. 2020 Mróz et al. (2020), the event rate observed in the northern hemisphere is lower than in the southern hemisphere. To examine the impact of this anisotropy, we consider the first-order perturbation of the density profile of MDMS:

$$\rho_{\text{aniso}}(x, y, z) = \begin{cases} (1 + \alpha)\rho_{\text{iso}}(x, y, z) & z > 0 \\ (1 - \alpha)\rho_{\text{iso}}(x, y, z) & z < 0 \end{cases} \quad (\text{A.6})$$

Here α is used to demonstrate the first-order anisotropy in the density profile

With this profile, we rerun the whole analyzing process with α as an additional parameter in the MCMC process. The result is shown in FIG. A.3. The result shows the density in the southern hemisphere is a little higher than the northern part ($\alpha = -0.008$), which coincides with the OGLE observation. Also, the new core size, 240 pc, is still within the one-sigma range shown in the main body of our paper. So, to the first-order level, the core size we present here is not significantly affected by the anisotropy.